optica

Sub-cycle optical control of current in a semiconductor: from the multiphoton to the tunneling regime

Tim Paasch-Colberg,[1,7] Stanislav Yu. Kruchinin,[1] Özge Sağlam,[2] Stefan Kapser,[1] Stefano Cabrini,[3] Sascha Muehlbrandt,[1] Joachim Reichert,[2] Johannes V. Barth,[2] Ralph Ernstorfer,[4] Reinhard Kienberger,[1,2] Vladislav S. Yakovlev,[1,5] Nicholas Karpowicz,[1] and Agustin Schiffrin[1,6,*]

[1]Max-Planck-Institut für Quantenoptik, Hans-Kopfermann-Str. 1, D-85748 Garching, Germany
[2]Physik-Department, Technische Universität München, James-Franck-Str., D-85748 Garching, Germany
[3]Molecular Foundry, Lawrence Berkeley National Lab, 1 Cyclotron Road, Berkeley, California 94720, USA
[4]Fritz-Haber-Institut der Max-Planck-Gesellschaft, Faradayweg 4-6, D-14195 Berlin, Germany
[5]Ludwig-Maximilians-Universität, Am Coulombwall 1, 85748 Garching, Germany
[6]School of Physics & Astronomy, Monash University, Clayton, Victoria 3800, Australia
[7]Current address: TOPTICA Photonics AG, Lochhamer Schlag 19, 82166 Graefelfing, Germany
*Corresponding author: agustin.schiffrin@monash.edu

Received 27 July 2016; accepted 9 October 2016 (Doc. ID 272365); published 14 November 2016

Nonlinear interactions between ultrashort optical waveforms and solids can be used to induce and steer electric currents on femtosecond (fs) timescales, holding promise for electronic signal processing at PHz (10^{15} Hz) frequencies [Nature 493, 70 (2013)]. So far, this approach has been limited to insulators, requiring extreme peak electric fields (>1 V/Å) and intensities (>10^{13} W/cm^2). Here, we show all-optical generation and control of electric currents in a semiconductor relevant for high-speed and high-power (opto)electronics, gallium nitride (GaN), within an optical cycle and on a timescale shorter than 2 fs, at intensities at least an order of magnitude lower than those required for dielectrics. Our approach opens the door to PHz electronics and metrology, applicable to low-power (non-amplified) laser pulses, and may lead to future applications in semiconductor and (photonic) integrated circuit technologies.

OCIS codes: (320.7130) Ultrafast processes in condensed matter, including semiconductors; (320.7100) Ultrafast measurements; (320.2250) Femtosecond phenomena; (270.6620) Strong-field processes; (270.1670) Coherent optical effects; (270.4180) Multiphoton processes.

http://dx.doi.org/10.1364/OPTICA.3.001358

Modern electronics relies on the control of electric current in solids [1]. The faster currents can be switched on and off in a device, the higher its performance. High electron mobility transistors [2] operate at ∼1 THz switching rates. Rates of ∼100 THz can be attained in semiconductors exposed to ultrashort laser pulses via photoconductive switching [3] and $\omega - 2\omega$ coherent control [4–9]. Recent experiments showed that currents can be generated and controlled in dielectrics at near-PHz frequencies via interactions with intense few-cycle optical fields [10–12]. This effect—a result of highly nonlinear phenomena within the limit of interband tunneling [13,14]—requires very high fields (>1 V/Å), limiting their potential applications.

Here, we demonstrate ultrafast, direct-field control of current at substantially lower fields in GaN, a material with a smaller bandgap ($E_g \approx 3.4$ eV), relevant for high-frequency and high-power (opto)electronics due to its electron mobility, mechanical stability, and heat capacity [15]. We show that charge displacement results from interference of multiphoton transitions [16] in the presence of field-induced intraband carrier motion and dynamic screening of the optical field. With increasing intensities, we observe a gradual transition from the multiphoton to the tunneling regime, supporting a unified quantum-mechanical picture valid in both limits.

We exposed the (0001) surface of wurtzite GaN to the waveform-controlled, linearly polarized visible/near-infrared (VIS/NIR) few-cycle laser pulses previously used in the prototypical study on silica [10] (see Supplement 1, Section 1). The instantaneous optical electric field, $F_L(t)$, was measured by attosecond streaking [17] in a parallel experiment [Figs. 1(a) and 4(b)]. The field was applied parallel to the surface, i.e., perpendicular to the permanent polarization of wurtzite GaN along its c-axis [18]. The stabilized carrier-envelope phase (CEP), φ_{CE}, was adjusted by varying the propagation length Δl inside a pair of fused silica wedges. We considered applied electric field peak amplitudes, F_0, up to 0.9 V/Å (cycle-averaged peak intensity, $I_0 \leq 10^{13}$ W/cm^2). Gold (Au) electrodes were patterned onto GaN, allowing for direct measurement of optically induced charge

displacements (i.e., time-integrated electric currents) in the material [Fig. 1(a) and Supplement 1, Section 2].

Figure 1(b) shows the CEP-dependent fraction Q_P of the charge per pulse collected by the unbiased Au electrodes as a function of Δl and $\Delta\varphi_{CE}$. Here, $F_L(t)$ was perpendicular to the electrodes along the x-axis [Fig. 1(a)]. The signal Q_P reverses its sign periodically with CEP. Inverting the optical field ($\Delta\varphi_{CE} = \pi$) reverses the direction of the charge displacement: the instantaneous electric field of the laser pulse is generated and controls Q_P, similar to the case of an insulator [10].

We measured $Q_P(\Delta l)$ for Au-GaN-Au junctions with inter-electrode distances of 100 nm, 5 and 10 μm at various field strengths. Within this electrode separation range, the maximum value of Q_P was given for 5 μm [4 ± 0.1 A fs $= (4 \pm 0.1) \times 10^{-15}$ Coulomb at $F_0 \sim 0.4$ V/Å; Fig. 1(b)]; for 100 nm and 10 μm, it was 1 ± 0.1 and 2.8 ± 0.1 A fs, respectively (both at $F_0 \sim 0.8$ V/Å). This hints at an optimal inter-electrode distance. A quantitative analysis of the maximum Q_P as a function of the junction size is beyond the scope of this study.

Figure 1(c) shows the CEP-optimized transferred charge, $Q_P^{(max)}$, as a function of F_0 and I_0, for junctions with 100 nm and 10 μm inter-electrode spacing. For $F_0 \le 0.45$ V/Å, the experimental data follow $Q_P^{(max)} \propto F_0^5$, independently of the junction size; this scaling law breaks down in larger fields. In comparison, data for SiO_2 from Ref. [10] shows a significantly higher order of nonlinearity and a breakdown of the power law scaling at a much stronger field ($F_0 \approx 1.7$ V/Å). Notably, for the same F_0 (e.g., ~0.9 V/Å), signals for GaN are at least two orders of magnitude larger than those for SiO_2.

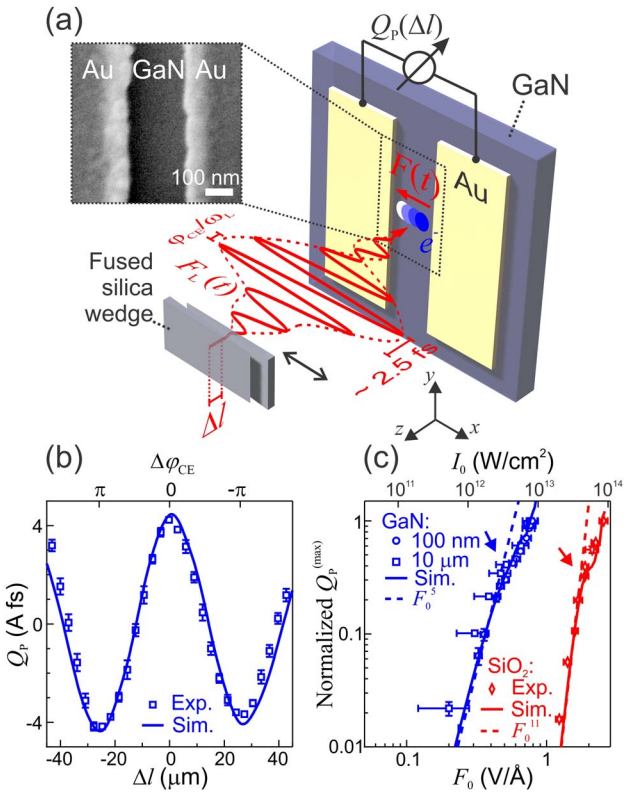

Fig. 1. (a) GaN surface patterned with gold electrodes (inset: SEM image) exposed to a CEP-controlled few-cycle VIS/NIR pulse with an instantaneous electric field, $F_L(t)$. Electrodes are unbiased. (b) CEP-dependent component Q_P of the collected charge per pulse as a function of propagation length Δl in the fused silica wedges and of the CEP change, $\Delta\varphi_{CE}$. Applied peak field amplitude, $F_0 = 0.4$ V/Å. Inter-electrode spacing: 5 μm. (c) Maximum Q_P (amplitude of sine fit of $Q_P(\Delta\varphi_{CE})$) as a function of F_0 and I_0 for 100 nm and 10 μm junctions. Data normalized with respect to values for maximum F_0. Data for SiO_2 [10] are shown for comparison. Arrows indicate breaking of the scaling power law. Solid curves: quantum-mechanical simulation.

When F_0 is varied, the transferred charge *shifts* with respect to $\Delta\varphi_{CE}$ [Figs. 2(b) and 2(c)], i.e., the charge-balancing CEP, $\varphi_{CE}^{(+0)}$, for which $Q_P(\varphi_{CE}^{(+0)}) = 0$, increases monotonically [Fig. 2(a)]. Here, we focus (arbitrarily) on the charge-balancing CEP related to the rising edge of $Q_P(\Delta\varphi_{CE})$, i.e., $\partial Q_P(\varphi_{CE}^{(+0)})/\partial\varphi_{CE} > 0$. The dependence of $\varphi_{CE}^{(+0)}$ on F_0 is not affected by the inter-electrode separation; it is an intrinsic characteristic of the material, as evidenced by the comparison with the SiO_2 case [12]; Fig. 2(a). The dependence $\varphi_{CE}^{(+0)}(F_0)$ allows for testing our theoretical model and aids the physical interpretation of our experiment.

Following the approach previously developed for SiO_2 [10], we decoupled *injection* (i) and *driving* (d) by exposing the junction to two synchronized, collinear VIS/NIR laser pulses with orthogonal electric fields $F_L^{(i)}(t)$ (parallel to electrodes, along y-axis; $F_0^{(i)} \approx 0.4$ V/Å) and $F_L^{(d)}(t)$ (perpendicular, along the x-axis, $F_0^{(d)} \approx 0.06$ V/Å); Fig. 3(a). The CEPs $\varphi_{CE}^{(i)}$ and $\varphi_{CE}^{(d)}$ of the respective fields were set according to the inset in Fig. 3(b), such that $Q_P(\Delta\varphi_{CE}) = 0$ in single-pulse experiments (as in Figs. 1 and 2). Figure 4(b) shows Q_P as a function of the delay Δt between the two pulses. For $\Delta t \approx 0$ fs, $Q_P(\Delta t)$ oscillates with a period of ~2.5 fs, i.e., the period of the optical field [Fig. 1(a)]. In Fig. 3(c), $\varphi_{CE}^{(d)}$ was changed by π; $F_L^{(d)}$ was reversed. Here, $Q_P(\Delta t)$ oscillates with the same period but is reversed in comparison to Fig. 3(b).

To clarify the physics behind the generated current, we compared our experimental data with quantum-mechanical (QM) simulations based on the numerical solution of the time-dependent Schrödinger equation [19] (Supplement 1, Sections 3–5). We considered optical transitions between three

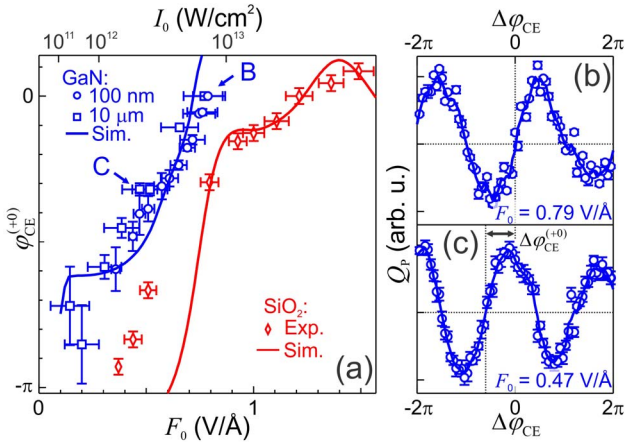

Fig. 2. (a) Charge-balancing CEP, $\varphi_{CE}^{(+0)}$, as a function of F_0 and I_0. Zero reference for $\varphi_{CE}^{(+0)}$ is set at $F_0 = 0.8$ V/Å. Data for SiO_2 are shown for comparison [12]. Solid curves: quantum mechanical simulation. (b), (c) $Q_P(\Delta\varphi_{CE})$ for $F_0 = 0.79$ [B in (a)] and 0.47 V/Å (C). Vertical dashed lines indicate the shift of $\varphi_{CE}^{(+0)}$ with F_0. Solid curves: smoothed experimental data.

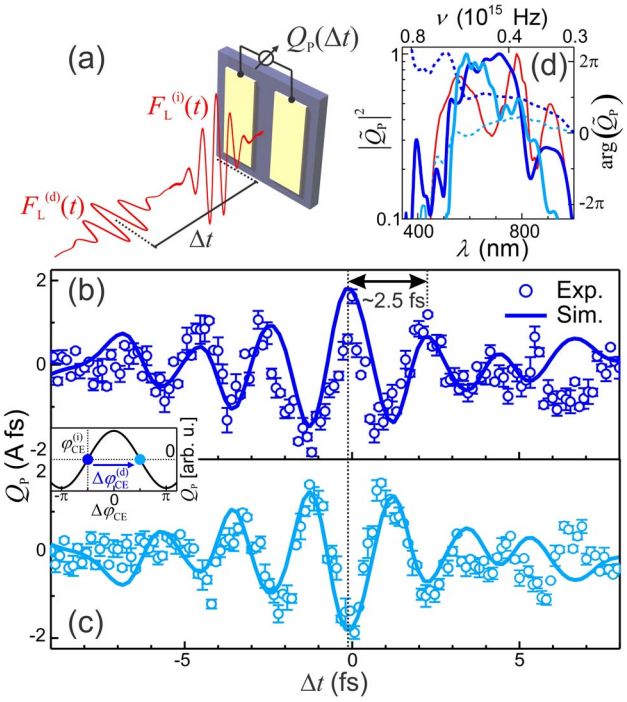

Fig. 3. (a) Injection-drive experiment. Two orthogonally polarized VIS/NIR laser pulses, delayed by Δt, irradiate a 5 μm Au-GaN-Au junction ($F_0^{(i)} \approx 0.4$ V/Å;$F_0^{(d)} \approx 0.06$ V/Å). $\varphi_{CE}^{(i)}$ and $\varphi_{CE}^{(d)}$ are set such that $Q_P(\Delta\varphi_{CE}) = 0$ when $F_L^{(i)}(t)$ and $F_L^{(d)}(t)$ are applied independently. (b) CEP-dependent component Q_P as a function of Δt. (c) Same as (b), with $\Delta\varphi_{CE}^{(d)} = \pi$. (d) Normalized modulus squared (solid) and phase (dashed) of the Fourier transform of $Q_P(\Delta t)$, $\tilde{Q}_P = \mathcal{F}[Q_P(\Delta t)]$, in (b) (blue) and (c) (cyan). Red: VIS/NIR pulse spectrum.

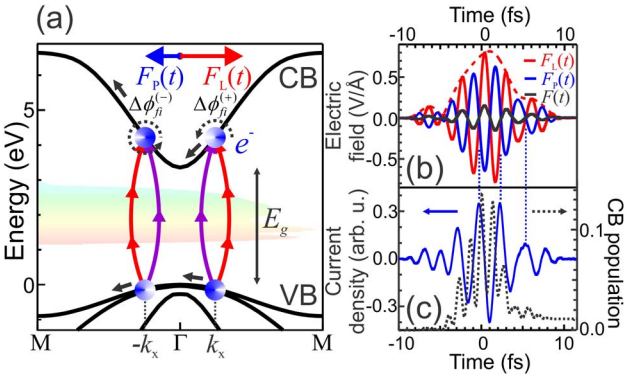

Fig. 4. (a) Current injection mechanism in GaN. Charge carriers are created via interfering two- and three-photon transitions between valence (VB) and conduction (CB) bands (blue circles: occupied states; white: unoccupied). Heavy hole, light hole, and crystal-field split-off VBs are shown. Background: laser pulse spectrum. Dynamic phase shifts (dashed black arrows) $\Delta\phi_{fi}^{(\pm)} \equiv \Delta\phi_{fi}(\pm k_x, t_1, t_2)$ resulting from field-induced intraband carrier motion (solid black arrows) determine whether interferences are constructive or destructive. (b) Applied optical electric field $F_L(t)$, induced polarization field $F_P(t)$ calculated with quantum mechanical dynamic screening model and total field $F(t) = F_L(t) + F_P(t)$. (c), Time-dependent current density $J(t)$ and electron population in the two lowest CBs calculated with quantum mechanical dynamic screening model.

valence (VB) and two conduction bands (CB) for crystal momenta k_x along the $\Gamma - M$ direction in the Brillouin zone (BZ) [Figs. 4(a) and S1 in Supplement 1]. The electrodes' orientations relative to the crystalline axes of the (0001) surface do not play an important role, since bands are isotropic in the vicinity of the Γ-point [20] and our field amplitudes are too low for most charge carriers to reach the BZ boundaries.

The theoretical curves (Figs. 1–3) are in good agreement with the experiments within the range of the considered field strengths. We interpret our results as follows. The interaction between GaN and the laser pulse induces a nonequilibrium asymmetrical population distribution in the VBs and CBs [Fig. 4(a)], leading to a CEP-dependent current along the optical field [5,21]. This asymmetric population is due to quantum interference of excitation pathways [16,21], which can be constructive for k_x and destructive for $-k_x$, or vice versa [see the calculated population distribution in Fig. S2c (Supplement 1), which is shifted from the BZ center and exhibits interference fringes]. The interference of the excitation pathways between electronic states in the initial and final bands with energies $E_i(k)$ and $E_f(k)$ is determined by the accumulation of dynamic phase [22]

$$\Delta\phi_{fi}(k_x, t_1, t_2) = \frac{1}{\hbar}\int_{t_1}^{t_2} \Delta E_{fi}[K_x(t)]\mathrm{d}t, \tag{1}$$

due to the intraband motion of electron-hole pairs between times t_1 and t_2 during exposure to the optical field. Here, $\Delta E_{fi}(k) = E_f(k) - E_i(k)$, $K_x(t) = k_x + eA(t)/\hbar$ is the semiclassical equation of intraband motion, $e > 0$ is the electron charge, and $A(t) = -\int_{-\infty}^{t} F(t')\mathrm{d}t'$ is the vector potential of the total electric field $F(t)$ in the Au-GaN-Au junction. For example, if, over an optical cycle, $\Delta\phi_{fi}(k_x, t_1, t_1 + 2\pi/\omega_L) = 2\pi N$ ($N = 1, 2, \ldots$), then contributions from different cycles interfere constructively and electron–hole pairs are efficiently excited. In the weak field limit, intraband motion can be neglected, $K_x(t) \approx k_x$, and $\Delta\phi_{fi} = 2\pi N$ yields the condition for absorbing N photons: $\Delta E_{fi}(k_x) = N\hbar\omega_L$. Resonances of different orders N can exist within an intense broadband pulse; their interference determines the asymmetry of k-space population distributions.

In the multiphoton regime, this quantum interference scenario yields a power-law scaling of the transferred charge $Q_P^{(max)} \propto F_0^{2N+1}$, where $N = \tilde{E}_g/\hbar\omega_L$ is the order of multiphoton interband transition and $\tilde{E}_g$ is the bandgap at a k-point where the corresponding transition is allowed [16] (Supplement 1, Section 6). The scaling power law $Q_P^{(max)} \propto F_0^5$ ($N = 2$) observed in the experiment and in the QM model for $F_0 \leq 0.45$ V/Å [Fig. 1(c)] shows that, within this field range, the charge displacement is triggered by a multiphoton process, consistent with our estimation of the Keldysh [14] parameter $\gamma_K \gtrsim 2$ (Supplement 1, Section 6).

For stronger fields, the slope of $Q_P^{(max)}(F_0)$ decreases and diverges from the F_0^{2N+1} scaling law. This is due to a combination of: (i) screening of the external field by the field-driven excited carrier displacement [23], and (ii) closing of the two-photon excitation channel [24] (Supplement 1, Section 6). The latter is a consequence of the ponderomotive energy becoming comparable to the photon energy, resulting in VB-to-CB transitions becoming nonresonant with the multiphoton process. This is indicative of

nonperturbative dynamics and a gradual transition from the multiphoton to the tunneling regime.

The field amplitude dependence of the charge-balancing CEP, $\varphi_{CE}^{(+0)}$ (Fig. 2), allows us to further test our QM model. The severe field-dependent shift of $\varphi_{CE}^{(+0)}$ is accurately reproduced by the theoretical curve. It is a direct consequence of the field screening due to the motion of charge carriers (Fig. S4, Supplement 1).

The measured $Q_P(\Delta t)$ (Fig. 3) resolves the oscillations of the optical field. Thus, it can be used for the implementation of a solid-state attosecond streak camera (see Supplement 1, Section 7). The spectrum of $Q_P(\Delta t)$ extends to a maximal frequency $f_{max} \sim 0.5$PHz, closely resembling the pulse spectrum [Fig. 3(d)]. According to the cross-correlation theorem, the carrier injection associated with each optical cycle cannot be confined to a time window significantly broader than $1/(2\ f_{max}) \sim 1$ fs, with significant contrast in the carrier excitation probability for adjacent optical cycles. The latter is ensured by the quasi-single-cycle character of the pulse and the nonlinearity of the process. Since the pulse duration is smaller than 4 fs, the current injection occurs within 2 fs. This is consistent with the recently observed nonlinear ultrafast carrier excitation in semiconductors [25,26].

In conclusion, we have demonstrated the injection and control of directly measurable currents in a semiconductor (GaN) on a timescale shorter than 2 fs. Our observations highlight the interplay between interfering multiphoton excitation channels and intraband carrier motion. As the latter becomes more significant, deviations from the perturbative scaling law become more severe. This indicates a continuous transition from the multiphoton to the tunneling regime and emphasizes the role of dynamic screening of the optical field inside the solid. Our findings pave the way for the development of ultrafast optically controlled solid-state electronics at intensities at least an order of magnitude smaller than those needed for an insulator. These intensities could further be decreased by optimizing junction geometries, opening the door to metrology for low-power (nonamplified) ultrashort laser pulse sources. Notably, this approach would leverage and further expand existing semiconductor and integrated circuit technologies.

Funding. Deutsche Forschungsgemeinschaft (DFG) Cluster of Excellence; Munich-Centre for Advanced Photonics (MAP); Max-Planck-Gesellschaft (MPG); Alexander von Humboldt Foundation; Swiss National Science Foundation (SNF); Marie Curie Fellowship (NANOULOP, 302157); European Research Council (ERC) (AEDMOS); Integrated Initiative LASERLAB-Europe; Australian Research Council (ARC) Future Fellowship; BaCaTeC; U.S. Department of Energy (DOE) (DE-AC02-05CH11231).

Acknowledgment. We thank Prof. F. Krausz for the helpful discussions, F. Scholz and K. Forghani for providing the GaN samples, and B. D. Harteneck for help in sample design and fabrication. Work at the Molecular Foundry was supported by the Office of Science, Office of Basic Energy Sciences, of the U.S. Department of Energy under Contract No. DE-AC02-05CH11231.

See Supplement 1 for supporting content.

REFERENCES

1. Y. Taur and T. H. Ning, *Fundamentals of Modern VLSI Devices* (Cambridge University, 1998).
2. R. Lai, X. B. Mei, W. R. Deal, W. Yoshida, Y. M. Kim, P. H. Liu, J. Lee, J. Uyeda, V. Radisic, M. Lange, T. Gaier, L. Samoska, and A. Fung, "Sub 50 nm InP HEMT device with Fmax greater than 1 THz," in *IEEE International Electron Devices Meeting (IEDM 2007)* (IEEE, 2007), pp. 609–611.
3. H. Shimosato, M. Ashida, T. Itoh, S. Saito, and K. Sakai, "Ultrabroadband detection of terahertz radiation from 0.1 to 100 THz with photoconductive antenna," in *Ultrafast Optics V* (Springer, 2007), pp. 317–323.
4. G. Kurizki, M. Shapiro, and P. Brumer, Phys. Rev. B **39**, 3435 (1989).
5. A. Hache, Y. Kostoulas, R. Atanasov, J. L. P. Hughes, J. E. Sipe, and H. M. Van Driel, Phys. Rev. Lett. **78**, 306 (1997).
6. L. Costa, M. Betz, M. Spasenovic, A. D. Bristow, and H. M. Van Driel, Nat. Phys. **3**, 632 (2007).
7. I. Franco, M. Shapiro, and P. Brumer, Phys. Rev. Lett. **99**, 126802 (2007).
8. I. Franco and P. Brumer, J. Phys. B **41**, 074003 (2008).
9. C. Ruppert, S. Thunich, G. Abstreiter, A. F. I. Morral, A. W. Holleitner, and M. Betz, Nano Lett. **10**, 1799 (2010).
10. A. Schiffrin, T. Paasch-Colberg, N. Karpowicz, V. Apalkov, D. Gerster, S. Muhlbrandt, M. Korbman, J. Reichert, M. Schultze, S. Holzner, J. V. Barth, R. Kienberger, R. Ernstorfer, V. S. Yakovlev, M. I. Stockman, and F. Krausz, Nature **493**, 70 (2013).
11. O. Kwon, T. Paasch-Colberg, V. Apalkov, B. K. Kim, J. J. Kim, M. I. Stockman, and D. Kim, Sci. Rep. **6**, 21272 (2016).
12. T. Paasch-Colberg, A. Schiffrin, N. Karpowicz, S. Kruchinin, O. Saglam, S. Keiber, O. Razskazovskaya, S. Muhlbrandt, A. Alnaser, M. Kubel, V. Apalkov, D. Gerster, J. Reichert, T. Wittmann, J. V. Barth, M. I. Stockman, R. Ernstorfer, V. S. Yakovlev, R. Kienberger, and F. Krausz, Nat. Photonics **8**, 214 (2014).
13. C. Zener, Proc. R. Soc. London Ser. A **145**, 523 (1936).
14. L. V. Keldysh, Sov. Phys. J. Exp. Theor. Phys. **20**, 1307 (1965).
15. S. Nakamura, S. Pearton, and G. Fasol, *The Blue Laser Diode: The Complete Story* (Springer, 2000).
16. S. Y. Kruchinin, M. Korbman, and V. S. Yakovlev, Phys. Rev. B **87**, 115201 (2013).
17. R. Kienberger, E. Goulielmakis, M. Uiberacker, A. Baltuska, V. Yakovlev, F. Bammer, A. Scrinzi, T. Westerwalbesloh, U. Kleineberg, U. Heinzmann, M. Drescher, and F. Krausz, Nature **427**, 817 (2004).
18. H. Morkoc, R. Cingolani, and B. Gil, Solid State Electron. **43**, 1909 (1999).
19. J. B. Krieger and G. J. Iafrate, Phys. Rev. B **33**, 5494 (1986).
20. M. Suzuki, T. Uenoyama, and A. Yanase, Phys. Rev. B **52**, 8132 (1995).
21. T. M. Fortier, P. A. Roos, D. J. Jones, S. T. Cundiff, R. D. R. Bhat, and J. E. Sipe, Phys. Rev. Lett. **92**, 147403 (2004).
22. M. S. Wismer, S. Y. Kruchinin, M. Ciappina, M. I. Stockman, and V. S. Yakovlev, Phys. Rev. Lett. **116**, 197401 (2016).
23. F. Della Sala, A. Di Carlo, P. Lugli, F. Bernardini, V. Fiorentini, R. Scholz, and J.-M. Jancu, Appl. Phys. Lett. **74**, 2002 (1999).
24. J. G. Story, D. I. Duncan, and T. F. Gallagher, Phys. Rev. A **49**, 3875 (1994).
25. H. Mashiko, K. Oguri, T. Yamaguchi, A. Suda, and H. Gotoh, Nat. Phys. **12**, 741 (2016).
26. M. Schultze, K. Ramasesha, C. D. Pemmaraju, S. A. Sato, D. Whitmore, A. Gandman, J. S. Prell, L. J. Borja, D. Prendergast, K. Yabana, D. M. Neumark, and S. R. Leone, Science **346**, 1348 (2014).